Journal of Materials Chemistry A

Accepted Manuscript

ROYAL SOCIETY OF CHEMISTRY

www.rsc.org/materialsA

Journal Name

ARTICLE

W^{6+} & Br^- Codoped $Li_4Ti_5O_{12}$Anode with Super Rate Performances for Li-Ion Batteries

Received 00th January 20xx,
Accepted 00th January 20xx

DOI: 10.1039/x0xx00000x
www.rsc.org/

Q. Y. Zhang,[a] H. S. Lu,[b] H. X. Zhong,[a] X. D. Yan,[a] C. Y. Ouyang*[b] and L. Z. Zhang*[a, b]

We report a novel $Li_4Ti_{5-x}W_xO_{12-x}Br_x$ (x=0.025, 0.050 and 0.100) anode material simultaneously doped with W^{6+} and Br^- ion prepared by a simple solid-state reaction in air, aiming to significantly improve its electrical conductivity of $Li_4Ti_5O_{12}$. Our theoretical calculation predicts that codoping with W^{6+} on the Ti^{4+} site and Br^- on the O^{2-} site can remarkably narrow down the band gap, and thus facilitates the electron transport in the lattice of LTO. The comparative experiments prove that W&Br-codoped LTO exhibits higher electrical conductivity compared with undoped LTO as expected, thus improved rate capability and specific capacity. Particularly, $Li_4Ti_{5-x}W_xO_{12-x}Br_x$ (x=0.05) exhibits the best rate capability and cyclic stability with an outstanding capacity retention of 88.7% even at 10 C rate after 1000 cycles. This codoping strategy with high valance transition metal and halide ions holds promise to be applied to other insulating cathode materials suffering from inferior electrical conductivity.

Introduction

Although the carbonaceous materials are widely employed as anode materials for lithium-ion batteries (LIBs), one of the serious drawbacks related with safety issue for these carbonaceous is their redox potentials similar to the lithium metal, which can readily form a dendritic structure during charge-discharge process and then cause a short-circuit inside the battery and potentially result in an explosion. [1]

As an alternative anode material for LIBs, LTO has attracted many considerable attentions due to its flat voltage plateau at around 1.55 V, which is much safer and more stable than carbonaceous materials, theoretical capacity of 175 $mAh{\cdot}g^{-1}$, high thermodynamic and structural stability with the zero-strain characteristics during charge and discharge process.[2] However, the untreated LTO typically shows poor rate performance due to its intrinsic low electrical conductivity (~10^{-13} $S{\cdot}cm^{-1}$),[3] which limits its application in LIBs, especially for the case that the rate performance is an important prerequisite such as electric vehicles.[4] To solve this problem, various strategies have been exploited, such as nanostructuring,[5-7] carbon coating,[8-10] and doping.[11-15] Among them, nanostructuring approach results in a very low power tap density and significantly decreases the volumetric energy density of LIBs,[16] while carbon coating method may not improve the electronic conductivity of LTO efficiently enough because of an incontinuous and/or excessively thick coated carbon layer.[17]

The doping method has been proved to be a direct and effective way to enhance the rate capability of LTO and some other cathode electrode materials suffering from similar poor electrical conductivity such as $LiFePO_4$.[18-20] However, most reports have mainly focused on solely doping at the Li, Ti or O site of LTO lattice.[21-24] These improvements are noteworthy but still insufficient for power-oriented applications. In order to significantly increase the electrical conductivity of LTO, La_{Li}-F_O,[25] Al_{Ti}-F_O,[26] Mg_{Li}-Zr_{Ti}[27] and Mg_{Li}-V_{Ti}[28] have been explored as codoping ions to substitute different sites such as tetrahedral 8a Li^+ site, 32e O^{2-} site and/or the octahedral 16d Ti^{4+} ($⅓Li^+$:$^5/_3Ti^{4+}$) site, and hence, breaking the charge balance due to unequal valences compared with corresponding substituted elements. As a result, some electrons will be generated to compensate the unbalanced charge, and the electronic conductivity is significantly improved, leading to enhanced rate capability. Therefore, codoping can greatly increase the electrical conductivity of LTO.

Of the possible transition-metal ion as a codopant, W^{6+} could be a good candidate, because higher-valence W may effectively generated more electrons by doing into bulk LTO.[29] Besides, substituted $[O]_{32e}$ with Br in the LTO spinel can also induce the formation of charge compensating Ti^{3+} (serving as electron donors) to increase conductivity.[30] Thus, codoping with W^{6+} and Br^- ions is a good strategy to improve LTO's electrical conductivity. Up to now, however, little attention has been paid to W&Br-codoping in spinel LTO anode material, though they are both common dopants solely used in LTO and has been shown to significantly improve its rate capability. Our density-functional theory (DFT) calculations reveal that doping LTO with the W&Br pair is the optimal choice because their orbitals are much lower in energy than that of corresponding substituted elements. E.g., the energy of Br 4*p* orbital is 5.0 eV, while the O 2*s* orbital in energy is 23.1 eV. So the Br atom

[a] *Key Laboratory of Renewable Energy, Guangzhou Institute of Energy Conversion, Chinese Academy of Sciences, Guangzhou 510640, PR China*

Email: qianyuzhang@ms.giec.ac.cn; 11110740020@fudan.edu.cn (Dr. Q. Y. Zhang); lzzhang@ms.giec.ac.cn (Dr. & Prof. L. Z. Zhang)

[b] *Department of Physics, Jiangxi Normal University, Nanchang 330022, PR China*

Email: cyouyang@hotmail.com (Dr .& Prof. C. Y. Ouyang)

*Corresponding authors: L. Z. Zhang and C. Y. Ouyang

energetically favors occupying O site (Br_O). This, of course, results in significantly lowering the conduction band and the energy of the system. Therefore, this W_{Ti}&Br_O- codoping can narrow the band gap and leads to dramatically enhanced electrical conductivity. In our previous work, W^{6+} doping was carried out to increase LTO's electronic conductivity, and then lead to the improvement of rate performance.[29] In addition, Qi et al. reported that Br-doping at O site was helpful in improving the electrochemical performances of LTO. An optimal composition of $Li_4Ti_5O_{12-x}Br_x$, x=0.2 improved the rate performance to a discharge capacity of 118 mAh·g^{-1} at 5 C and 100 mAh·g^{-1} at 10 C.[31] Therefore, we expect that W&Br-codoping can be utilized to further enhance the electrochemical performance, as the so-called "synergistic effect". Since most previous studies have focused on investigating the codoping phenomena themselves, like the variations of electronic conductivity and electrochemical properties, the fundamental origin of such phenomena is still not fully understood. In this work, we also revealed the modification mechanism of W^{6+} & Br^- codoping by first-principles calculations based on DFT.

Experimental

Materials preparation and characterization

$Li_4Ti_{5-x}W_xO_{12-x}Br_x$ (x= 0, 0.025, 0.05, and 0.10) samples were synthesized by a solid-state reaction using stoichiometric amounts of Li_2CO_3, TiO_2, $WO_3$and LiBr as Li, Ti, W and Br sources, respectively. Firstly, the raw materials were mixed by ball milling for 5h, and then calcined at 800℃ for 12h in a furnace under air atmosphere. 5% excess Li was provided to compensate for the evaporation at high temperature during synthesis.

The final stoichiometry of the W&Br-codoped LTO composite was confirmed by composition analysis. The content of Br^-ion was analyzed using anion selective electrode, and the content of Ti was determined by titration with EDTA while the determination of $W^{6+}$and Li^+ were analyzed by inductive coupled plasma optical emission spectroscopy (ICP-OES, Varian Vista MPX) and thus, to estimate their stoichiometry.

The electrode materials for SEM characterization after cycling to confirm the structural stability were obtained through the processes as shown in Fig. 1S. NMP was used to separate the anode materials from AI foil. A thermal treatment was necessary to eliminate acetylene black and PVDF binder in the anodic active materials. The W&Br codoped-LTO materials from lithium-ion battery after 200 cycles were then calcined at 750℃ for 5h in a muffle and cooled to room temperature(25℃).

XRD analysis employing Cu *Kα* (10°≤2ϑ≤80°) radiation with a scan rate of 0.02°·s^{-1} was used to identify the crystalline phase of the as-prepared powders (PANALYTICAL Incorporated, Netherlands). Particle morphologies and sizes of the samples were observed by SEM (Hitachi S-4800, Japan) with an energy-dispersive detector (EDS). Raman spectra of all samples were obtained on a HR800 Confocal Raman spectroscopy (HORIBA Jobin Yvon, France) with a 532 nm laser source.XPS measurements and analyses were carried with an ESCALAB 250Xi system (USA).

Battery preparation

The experimental batteries were assembled at room temperature in an Ar-filled glove box, with the water content less than 0.1 ppm. Electrode sheets were prepared by mixing 80 wt% active material (pristine LTO or codoped LTO), 10 wt% carbon black, and 10 wt% polyvinylidene fluoride binder (PVDF) dissolved in N-methyl pyrrolidone (NMP) in a mortar to form a homogeneous slurry, which was spread onto cleaned Al foil using the doctor blade technique, and then dried at 120℃ for 10 h under vacuum. The obtained electrode was punched into disks, which were used as the working electrodes. The thickness of as-prepared electrodes is about 10 μm and the active loading mass was roughly 2.5 mg per electrode. These anodes were assembled into CR2025 coin cells. Li foil was used as the counter and reference electrodes, while using 1M $LiPF_6$-EC/DEC/DMC (1:1:1, in volume) as the electrolyte and Celgard 2400 microporous polypropylene membrane as the separator. Before electrochemical testing, the batteries were allowed to rest for 24 h to ensure sufficient soakage.

Electrochemical measurement

Electrochemical tests were carried out by using the above mentioned CR2025 coin cells. Galvanostatic cycling tests were conducted in the voltage range of 1.0-2.5V (*vs*. Li/Li^+) at various currents rates from0.1to 20 C. For cyclic performance measurements, the current was varied from 1 C to 10 C. Cyclic voltammetry (CV) was measured on a Zennium/IM6 electrochemical workstation (Zahner, Germany) between 1.0 and 2.5 Vat a scanning rate of 0.5 and 5 mV·s^{-1}. Electrochemical impedance spectroscopy (EIS) measurements were also measured at the electrochemical workstation with a ±5 mV AC signal and a frequency range from 10 mHz to 100 kHz. All experiments were carried out at room temperature (25℃).

Computational details

All the calculations in the present studies are performed in the framework of density-functional theory using the Vienna a b initio simulation package (VASP).[32] This package has been proved to be suitable for predicting the crystalline and electronic structures of spinel LTO by the generalized gradient approximation (GGA) and pseudo potential framework.[33, 34] The Perdew-Burke-Ernzerhof (PBE) was used for the calculation of the electron exchange correlations energy.[35]

The convergence tests of the total energy with respect to the k-points sampling and the cut-off energy were carefully examined. A gamma point mesh with 3×3×3k-points was specified in the Brillouin zone and periodic boundary conditions were utilized on the model systems. The atomic positions, lattice parameters and cell volume are fully relaxed to simulate the optimized structure of each lattice model, with a cutoff energy of 580 eV on a plane wave basis set. The total energies are converged better than 10^{-5} eV, and the final force on each atom is less than 0.02 eV/Å(1 Å= 0.1 nm). For all the DOS calculations, The Gaussian smearing method is used and the broadening width is 0.05 eV.

Results and discussion

On the basis of chemical analysis, the final chemical formula of the W^{6+}&Br^-- codoped LTO were determined as shown in Table 1. It can be seen that final formula of codoping LTO samples are almost in accordance with their nominal formula, though part of bromum was lost due to their volatilization during the synthesis at high temperature.

Fig. 1(a) shows the XRD patterns of the $Li_4Ti_{5-x}W_xO_{12-x}Br_x$ (x= 0, 0.025, 0.05, 0.10). All the four samples show the major peaks of

cubic LTO(JCPDS No. 49-0207), and no impurity peaks can be detected, indicating that the W^{6+} and Br^- ions have successfully entered the lattice structure of LTO bulk without causing any changes or forming a new phase. A representative refinement when x=0.05 is shown in Fig. 1b. All the peaks are sharp and well defined, indicating that the crystallinity of the compound is high. The refinement is in a good agreement with the spinel phase. Additionally, as shown in the inset of Fig. 1(a), the colors of different codoped samples are distinct. When x=0.025, it remains white as the color of pristine LTO. However, the color of the samples when x=0.05 and 0.10 are yellow and brown, respectively. A simple mixture of LTO,$WO_3$and LiBr cannot show such uniform color, which deepens with increasing codoping amount, suggesting that W^{6+} and Br^- would have reacted with LTO to form a lattice-codoped phase of LTO with a changed color. The optical and electrochemical properties of LTO are therefore altered by the codoping method.

According to the enlarged peak of (111) planes of the samples shown in Fig. 1(b), it can be observed that the codoped samples undergo a slight shift toward lower degrees, indicating that the lattice parameter of LTO increases with the increasing codoping amount. The lattice parameter of$Li_4Ti_{5-x}W_xO_{12-x}Br_x$ (x= 0, 0.025, 0.05, 0.10) samples are shown in Table 2. The '*a*' value of undoped LTO is 0.8357 nm, which is in a good agreement with literature data reported by Deschanvres.[36] The lattice parameter increases upon W^{6+}&Br^-codoping level from 0.8357 to 0.8375nm, as x increased from 0 to 0.10.This trend can be explained by the fact that the difference of radius between Br^- and O^{2-} is much more than that between W^{6+} and Ti^{4+}.The radius of Ti^{4+}, W^{6+}, O^{2-} and Br^- ions are as following: R_{Ti}^{4+} =0.0605 nm, R_W^{6+}=0.060 nm, R_O^{2-} =0.14 nm, and R_{Br}^- =0.196 nm, respectively. Moreover, the codoping of W^{6+} and Br^- will cause the transition of a certain amount of Ti^{4+} to Ti^{3+} as charge compensation. As the ionic radius of Ti^{3+} (0.067 nm) is larger than that of Ti^{4+} (0.0605 nm), its effect also increases the lattice parameter. Thus, as a whole result, the lattice parameter extends with the codoping of W^{6+} and Br^- ions, which facilitates the Li^+ ions insertion and extraction processes without lattice stability damaged.[37]

The Raman spectra of the $Li_4Ti_{5-x}W_xO_{12-x}Br_x$ ($0 \le x \le 0.10$) samples are shown in Fig. 2. It can be seen that five vibration peaks were observed at 233, 348, 419, 670 and 748 cm^{-1}, which are the feature of the spinel structure ($A_{1g}+E_g+3F_{2u}$).[38] The frequencies in the 600-800 cm^{-1} region are assigned to Ti-O stretching vibrations in "TiO_6"octahedral, and the frequencies of the Li-O stretching vibrations in "LiO_6"octahedral are known to lie in the 250-400 cm^{-1} region. Whereas the major peak in the 400-600 cm^{-1} rang corresponds to the Li-O band vibration in "LiO_4"tetrahedral.[39, 40]This observation demonstrates that the modification ofW^{6+}&Br^--codoping cannot change the vibration characteristic and basic spinel structure of LTO. Furthermore, it can be found that the Raman peak intensity decreases substantially in codoped LTO with respect to the undoped sample. It has been reported that the Raman signal intensity decreases as particle size increases,[41] which is well consistent with the aforementioned XRD results. Therefore, the codoped samples may have a relative bigger particle size than that of pure LTO.

Fig. 3 shows SEM images of W^{6+}&Br^--codoped and undoped LTO powders. It is apparent that the morphologies of the as-prepared powders are similar. All materials are well crystallized with a uniform particle size distribution in the range of 0.6-1.3 μm. The average particle size is about 1.0 μm.

In order to see if the codoped elements are uniformly dispersed in LTO bulk, we analyzed the elemental mapping of the $Li_4Ti_{4.95}W_{0.05}O_{11.95}Br_{0.05}$ sample by EDS measurement. Fig. 4 exhibits the distributions of the element O, Ti, W and Br in the tested area (SEM image in Fig. 5), respectively. The presence of these four elements is verified by the EDX result shown in Fig. 5. It can be seen from Fig. 4 that all the elements have homogeneous distributions, demonstrating that the $W^{6+}$and Br^-were uniformly doped into LTO crystal structure via the solid-stated reaction. This process can be shown by the following chemical reaction:

$$W^{6+} + Br^- \xrightarrow[Li_4Ti_5O_{12}]{\text{codoping}} W_{Ti}^{''} + Br_O^{'} + 3e^{\bullet} \quad (1)$$

Based on the above Eq. 1, substitutions of W^{6+} for Ti^{4+} and Br^- for Li^+ will create Ti^{4+} vacancy ($W_{Ti}^{''}$) and O^{2-} vacancy ($Br_O^{'}$) in the lattice of LTO, respectively. The generated vacancies induce partial reduction of Ti^{4+} to Ti^{3+} for charge compensation. To obtain the detailed information about the content of Ti^{3+} in the Ti atoms, the XPS characterizations corresponding to the Ti2p spectra were measured for these four samples. Fig. 2S(a) showed two peaks at 464.8 and 459.1 eV, which correspond to the $Ti2p_{1/2}$ and $Ti2p_{3/2}$ core level binding energy of Ti^{4+}, respectively. The presence of Ti^{3+} in the W&Br-codoped samples was further supported by a pair of new Ti 2p peaks observed at 458.6 and 463.2 eV as shown in Fig. 1S(b-d). Ti^{3+} content was analyzed as 4.47%, 9.65% and 18.73% through the peak areas, respectively. Ti^{3+} content increases with increasing codopant from 0.025 to 0.010. The results promote the reduction of Ti^{4+} to Ti^{3+} to balance the charge. In order to further prove the presence of Ti^{3+} ions in W&Br-codoped LTO, the XPS spectra of $Li_4Ti_{5-x}W_xO_{12-x}Br_x$ materials when x=0 and x=0.05 were comparatively studied, and their survey spectra are shown in Fig. 6a, which identifies strong signals of Li, Ti and O in pure and codoped LTO samples. In addition to these three elements, W and Br elements were also detected in the $Li_4Ti_{4.95}W_{0.05}O_{11.95}Br_{0.05}$sample. As shown in Fig. 6a, very weak signals for W and Br elements were detected for $Li_4Ti_{5-x}W_xO_{12-x}Br_x$, x = 0.05 due to their low codoping contents. The C 1s peak can be clearly observed on the surface of $Li_4Ti_{5-x}W_xO_{12-x}Br_x$ (x = 0, 0.05) powders, which was used for calibration. In Fig. 6b, the pristine and codoped LTO samples exhibited characteristic two sets of spin-orbit doublets of Ti $2p_{1/2}$ (464.9 eV) and $Ti2p_{3/2}$ (459.1 eV), which were assigned to Ti^{4+} oxidation state.[42] The peak separation between the Ti $2p_{1/2}$ and Ti $2p_{3/2}$ lines(ΔTi-2p = $2p_{1/2}$ - $2p_{3/2}$)was 5.8 eV, which was also consistent withTi^{4+} oxidation state. Another pair of smaller peaks in the XRD pattern of $Li_4Ti_{4.95}W_{0.05}O_{11.95}Br_{0.05}$ sample that located at 464.5 and 458.7 eV belongs to Ti $2p_{1/2}$ and Ti $2p_{3/2}$, respectively. Compared with the XPS spectrum of undoped LTO, a noticeable shift ($\Delta\delta$=0.4eV) can be observed, indicating the existence of Ti^{3+}in the $Li_4Ti_{5-x}W_xO_{12-x}Br_x$, x = 0.05 powder. Thus, after codoping of W^{6+} and Br^-, it can result in the presence of mixed Ti^{3+}/Ti^{4+} ions. Both of the codoping ions were attributed to the reduction of valence state of Ti cations from Ti^{4+} to Ti^{3+}. The conversion of Ti from higher-valence state (+4) to lower-valence state (+3) is always accompanied by the generation of electrons to compensate charge balance, and subsequently results in the improvement of electronic conductivity. Therefore, it can be inferred that the W&Br-codoping may enable the $Li_4Ti_{5-x}W_xO_{12-x}Br_x$,

x=0.05sample to present a better electrochemical performance, especially rate capability.

To demonstrate the effect of W&Br-codoping on improving the rate capability of the electrodes, the cyclic performance of the $Li_4Ti_{5-x}W_xO_{12-x}Br_x$(x=0, 0.025, 0.050 and 0.100) samples at different current rates is shown in Fig.7. For each stage, the charge-discharge processes of the samples were subject to 10 cycles. It can be clearly seen that undoped LTO sample exhibits high discharge capacities and good cycling stabilities at 0.1 C, its initial discharge capacity is 169.5 $mAh{\cdot}g^{-1}$. However, its capacity decreases dramatically as current rate increases, while the codoped samples display relatively higher capacity. At 1 C, 5 C, 10 C and 20 C, the capacities of pure LTO are133.2 $mAh{\cdot}g^{-1}$, 113.5 $mAh{\cdot}g^{-1}$, 80.2 $mAh{\cdot}g^{-1}$, 44.6 $mAh{\cdot}g^{-1}$, respectively. Better electrochemical performances for W&Br-codoped LTO materials were found upon increasing the charge-discharge rate. Among all doped samples, the $Li_4Ti_{5-x}W_xO_{12-x}Br_x$,x = 0.05 shows the best rate capability. Its specific capacity exceeds the pristine LTO following a rate of 0.5 C. At 1 C, 5 C and 10 C, the capacities are 160.0$mAh{\cdot}g^{-1}$, 151.3$mAh{\cdot}g^{-1}$ and 139.5$mAh{\cdot}g^{-1}$, respectively. Even at 20 C, its capacity still remains 120.8 $mAh{\cdot}g^{-1}$, which is 70.7% of the initial discharge capacity at 0.1 C. On the other hand, pristine LTO shows much lower capacity – only 26.3% of that at 0.1 C. Moreover, as the current rate returned to 0.1 C after 60 cycles, a stable capacity of170.5 $mAh{\cdot}g^{-1}$ can be obtained without any decay in the following 10 cycles. These results demonstrate that the $Li_4Ti_{5-x}W_xO_{12-x}Br_x$ electrode has an excellent reversibility and stability.

The cyclic performances of $Li_4Ti_{5-x}W_xO_{12-x}Br_x$ (x=0, 0.025, 0.050 and 0.100) at the rates of 1 C, 5 C, and 10 C are shown in Fig.8. Seen from Fig. 8a and b, it is obvious that the discharge capacity of $Li_4Ti_{5-x}W_xO_{12-x}Br_x$,x = 0.05is much higher than that of other samples at 1 C and 5 C rates. When discharged at 1 C and 5 C after 200 cycles, its capacities are 158.8 $mAh{\cdot}g^{-1}$ and 149.0 $mAh{\cdot}g^{-1}$, respectively. Fig.8c shows thatthe discharge capacity can still reach 138.8 $mAh{\cdot}g^{-1}$ and maintain 88.7% of its initial discharge capacity over 1000 cycles even at 10 C rate, which is much higher than that of solely doped LTO electrodes.On the other hand, pure LTO electrode decreased to 80.6 $mAh{\cdot}g^{-1}$only after 200 cycles at 10 C.In sum, the W&Br-codoped LTO samples have higher capacity than that of undoped LTO at the same discharge current rate. In addition, $Li_4Ti_{5-x}W_xO_{12-x}Br_x$electrode shows excellent capacity retention. When the amount of W&Br-codoping is higher than x=0.05, however, the capacity decreases. Thus, the x=0.05codopant amount is most appropriate.

The initial charge-discharge curves of the electrodes prepared from pristine LTO and$Li_4Ti_{5-x}W_xO_{12-x}Br_x$, x=0.05 powders were measured at different current rates, as shown in Fig. 9.We can clearly see that the discharge voltage plateau drops when the current rate increases, for both electrodes. The discharge plateau of the pristine LTO was 1.55 V at 0.1 C. Upon increasing current, however, the overpotential was observed to dramatically increase, relative to the $Li_4Ti_{5-x}W_xO_{12-x}Br_x$ electrode when x=0.05. For the $Li_4Ti_{5-x}W_xO_{12-x}Br_x$, the discharge plateau was also 1.55 V, but did not decrease as quickly as LTO, when the current rates increased. Both pristine LTO and $Li_4Ti_{5-x}W_xO_{12-x}Br_x$, x=0.05 reached near the theoretical discharge capacity of 175 $mAh{\cdot}g^{-1}$, being 170.3 $mAh{\cdot}g^{-1}$ and 173.3 $mAh{\cdot}g^{-1}$ at 0.1 C, respectively. At 20 C, however, the capacity of the latter is 117.5 $mAh{\cdot}g^{-1}$, while that of the former is only 44.6 $mAh{\cdot}g^{-1}$. Accompanying the lower capacity of pristine LTO was more polarization of the plateau. The polarization or gap between discharge and charge plateaus widens only slightly for $Li_4Ti_{5-x}W_xO_{12-x}Br_x$, x=0.05, compared to the pristine material. To demonstrate this further, the inset in Fig. 8c shows the charge-discharge curves of pure LTO at 200th cycle and $Li_4Ti_{5-x}W_xO_{12-x}Br_x$ (when x=0.05) at 1000th cycle, respectively. It can be seen that the gap between charge and discharge plateau of the former anode is almost two times larger than that of the following anode, i.e., $\Delta E_1 = 3\Delta E_2$. Therefore, the polarization of pristine LTO is more than that of $Li_4Ti_{5-x}W_xO_{12-x}Br_x$, x=0.05. In order to explain this phenomenon, Fig.10 shows the CV of each material at scan rates of 0.5 $mV{\cdot}s^{-1}$ and 5 $mV{\cdot}s^{-1}$ within a sweep voltage range of 1-2.5 V (vs. Li/Li^+), corresponding to very low and high C-rates, respectively. All samples show a pair of sharp and reversible redox peaks at each scan rate, indicating the good electrode kinetics of all anodes. The potential difference (ϕ_a-ϕ_c) between anodic and cathodic peaks can reflect the degree of polarization of the electrode.[43] From Table 3, it can be seen that the potential difference of all codoped LTO electrodes is lower than that of pure LTO, though it exhibits smaller polarization at lower scan rate of 0.5 $mV{\cdot}s^{-1}$, suggesting that the W & Br-codoping enhanced the reversibility of the LTO. Among all samples, $Li_4Ti_{5-x}W_xO_{12-x}Br_x$,x=0.05shows the least potential difference under the same current rate, indicating that too high an amount of codoping is adverse. Thus, the optimal degree of W&Br-codoping is x=0.05. This result is in agreement with the galvanostatic charge-discharge analysis given earlier.

The rate-capability of LTO is mainly determined by electronic and lithium-ionic conductivities. To evaluate the enhancement of electronic conductivity due to the codoping with W^{6+} and Br^- ions, EIS measurements were carried out for the $Li_4Ti_{5-x}W_xO_{12-x}Br_x$ (x=0, 0.025, 0.050 and 0.100) electrodes at the voltage of 1.55 V after the first cycle. Fig. 11a shows the Nyquist plots obtained from the spinel $Li_4Ti_{5-x}W_xO_{12-x}Br_x$ (x=0, 0.025, 0.050 and 0.100) electrodes, while the inset is the corresponding equivalent circuit used in analysis. All the EIS curves are composed of a depressed semicircle at the high to intermediate frequency range, and a straight line in the lowest frequency region. The high frequency semicircle is related to the charge transfer resistance at the active material interface, while the sloping line at the low frequency end indicates the Warburg impedance caused by a semi-infinite diffusion of Li^+ ion in the electrode. In the equivalent circuit, R_s is the ohmic resistance of electrolyte; R_{ct} is the charge transfer resistance; CPE is a constant phase element used to represent the double layer capacitance and passivation film capacitance; Z_w represents the Warburg impedance.[26,44] Table 4 shows that the charge transfer resistance (R_{ct}) of W&Br-codoped electrodes are much lower than that of the pure LTO, indicating that this codoping reduces the resistance, enhancing the charge transfer across the electrode-electrolyte interface. Herein, $Li_4Ti_{5-x}W_xO_{12-x}Br_x$, x=0.05 exhibits the least charge transfer resistance among all samples. In conjunction with the analysis above, it is reasonable to infer that this lowest R_{ct} value corresponds with the material's smallest electrochemical polarization, thus leading to the best cyclic performance at high charge-discharge rate.

The diffusion coefficient (*D*) of lithium ion can be calculated from the plots in the low-frequency region (Fig. 11b). The straight lines are attributed to the diffusion of the lithium ions into the bulk of the electrode materials, the so-called Warburg diffusion. We can obtain the value of *D* according to the following equations:

$$Z_{re}=R_s+R_{ct}+\sigma_w{\cdot}\omega^{-1/2} \quad (2)$$

$$D = 0.5\left(\frac{RT}{AF\sigma_\omega C}\right)^2 \quad (3)$$

Where ω is the angular frequency in the low frequency region; σ_w is the Warburg impedance coefficient; *D* is the diffusion coefficient; R is the gas constant; T is the absolute temperature; F is Faraday's constant; A is the area of the electrode surface; and C is the molar concentration of Lithium ions (moles·cm^{-3}).[45] The impedance parameters are recorded in Table 4.As mentioned above, the enlarged lattice constant due to W&Br-codoping is beneficial for fast Li^+ transfer, and thus improving its diffusion coefficient *D*. It can be seen that the W&Br-codoped$Li_4Ti_{5-x}W_xO_{12-x}Br_x$ (x=0.025, 0.05, 0.10) electrodes have better diffusion coefficients than the LTO electrode without codoping. The $Li_4Ti_{5-x}W_xO_{12-x}Br_x$, x = 0.05 electrode presents the highest lithium diffusion coefficient, which is favorable for rapid charge and discharge, indicating that the selection of an appropriate amount of codopants is very important.

For the above mixed ionic and electronic conductor, the ionic conduction and electronic conduction are not two independent processes, which are influenced and limited by each other. The total conductivity of electrode can be expressed by: [46]

$$\sigma_t = \frac{\sigma_i \sigma_e}{\sigma_i + \sigma_e} \quad (4)$$

Where σ_t is the total conductivity, σ_i is the ionic conductivity and σ_e is the electronic conductivity. For the investigated system of $Li_4Ti_{5-x}W_xO_{12-x}Br_x$, the electronic conductivity will be enhanced by codoping with W^{6+} and Br^- ions due to the generation of mixing Ti^{4+}/Ti^{3+} for charge compensation, and the Li-ion conductivity may increase owing to the enlarged lattice parameter that is favorable for Li-ion transportation. Based on Eq. 4, as a function of σ_i and σ_e, the total conductivity of electrode material is a monotonic increasing function. The σ_t monotonously increases as σ_i and σ_e increase. As shown in Table 4, the $Li_4Ti_{5-x}W_xO_{12-x}Br_x$, x=0.05 electrode has the best electronic conductivity and ionic conductivity. Therefore, σ_t reaches its maximum value when x=0.05. That is why $Li_4Ti_{5-x}W_xO_{12-x}Br_x$, x = 0.05 electrode exhibits the best rate capability.

It can be explained in terms of $Li_4Ti_{5-x}W_xO_{12-x}Br_x$, x =0.05 with the highest electrical conductivity that leads to best rate performance. Fig. 3S reveals the variations of the electronic conductivity and Li^+ diffusion coefficient as functions of the composition x (shown in the below). By the results of the four-point probe meter, the electrical conductivity of the W&Br-codoped LTO was greatly improved. It can be observed that the x=0.05 sample exhibits much higher electronic conductivity than other samples, especially almost improved 6 orders of magnitude compared with pristine LTO, which cannot be measured by the four-point probe method. The enhanced electrical conductivity can be explained by the synergistic effect of W&Br-codoping. For $Li_4Ti_{5-x}W_xO_{12-x}Br_x$ (x=0.025, 0.050 and 0.100) samples, W^{6+} and Br^- partially substituted Ti^{4+} and O^{2-} sites of LTO, respectively. This codoping breaks the charge balance in LTO, and subsequently generated Ti^{3+} for charge compensation. This can be explained by the best combination of the lattice parameter of Br^- in O^{2-} site and the occupancy of W^{6+} in Ti^{4+} site. The dopant Br^- herein plays a dominant role in lattice parameter. It is well known that Li^+ ions transport in three-dimensional pathways during lithiation/ delithiation processes in the spinel LTO bulk. Li^+ ions have to pass through the O^{2-} ion planes located between the octahedral and tetrahedral sites, which form a transportation bottlenecks. The large parameter mainly caused by Br-doping increases the transfer distance of Li^+ between the neighboring O^{2-} ions. Correspondingly, the Li-ion diffusion coefficient decreases with increasing Br^- content. Besides, W^{6+} located at octahedral 16d sites after doping. Increasing x will result in more inaccessible octahedral vacancies and thus less Li^+ ions in the octahedral vacancies over cycling and more on the tetrahedral vacancies. Since the hysteresis is largely ascribed to the lithiation/delithiation in the tetrahedral vacancies, the hysteresis becomes larger when x equals 0.1. We can see clearly from Fig. 8b that the discharge capacity of x=0.1 is obviously decreased compared with the x=0.05 at 5 C rate after 200 cycles. Therefore, $Li_4Ti_{5-x}W_xO_{12-x}Br_x$, x=0.05 sample exhibits the best compromise in terms of the highest electronic conductivity and Li^+ diffusion coefficient among all codoped samples.

SEM characterization was carried out to investigate the structure stability of W&Br-codoped LTO materials after long cycles. It can be seen from Fig. 4S that all of the codoped samples exhibited a spinel shape with a particle size in the range of 0.6-1.3 μm and relatively uniform morphology. No obvious change was observed compared with initial synthesized samples, indicating that W&Br-codoping did not affect LTO's structural stability after cycling.

In order to further elucidate the electronic and structure changes of W & Br-codoped LTO materials, DFT calculations were used to calculate energetically optimized lattice models of the pristine, W and Br solely doped and codoped LTO. Firstly, to satisfy the stoichiometry of $Li_4Ti_5O_{12}$, the structural model containing 2 formula units is built from the unit cell of $Li_4Ti_5O_{12}$ through the following transformation matrix: [0.5 1 0.5; 0.5 -0.5 0.5; 1 0.5 0]. Twelve 16d sites exist in the model, and two of them are occupied by Li according to the ratio of Li to Ti at this lattice site. Thus, we use a 1×1×2 super cell of the structural model for calculations. Those structures are represented in Fig. 12.

In order to investigate the effect of W & Br-codoping upon the enhanced electrochemical performances of $Li_4Ti_5O_{12}$, we utilize a DFT band structure calculation on $Li_4Ti_5O_{12}$ and $Li_4Ti_{4.75}W_{0.25}O_{11.75}Br_{0.25}$ ($Li_{16}Ti_{19}W_1O_{47}Br_1$), as shown in Fig.13a&b, respectively. The band gap of pristine $Li_4Ti_5O_{12}$ is about 2.3 eV, which is mainly determined by the Ti 3d and O 2p bands, indicating that $Li_4Ti_5O_{12}$ is a typical insulator.[24] In Fig. 13a, however, the projected DOS of $Li_4Ti_{4.5}W_{0.5}O_{11.5}Br_{0.5}$is moved downwards with respect to the normalized energy ($E-E_f$), and the tail of conduction bands is placed below the Fermi level, becoming partly filled. This suggests that only little energy is necessary for an electron to move to an energy level higher than the Fermi level. Remarkably, this codoping case demonstrates that W & Br-codoped $Li_4Ti_5O_{12}$ is an electrical conductor with increased rate capability.

In the present work, we have shown that W & Br-codoped LTO leads to significantly improved electrical conductivity and therefore greatly enhanced electrochemical performance as compared to undoped LTO. The underlying reason is that the codoping modifies the nature of the binding energy minimum so that the modification mechanism is changed to more favorable electron conduction. The electrochemical kinetics was shown to improve in terms of polarization and charge transfer resistances, as well as lithium ion diffusion and even capacity retention. The results summarized here indicate that $Li_4Ti_{5-x}W_xO_{12-x}Br_x$, x = 0.05is a particularly promising anode material with excellent rate capability, cycling stability, and

reversibility. Importantly, this charge-compensated codoping can be applied to improve the rate performance of other cathode materials suffering from inferior electrical conductivity.

Conclusions

$Li_4Ti_{5-x}W_xO_{12-x}Br_x$(x=0.025, 0.050, 0.100) samples were successfully synthesized by a simple solid-state reaction in air atmosphere.XRD patterns demonstrated that W &Br-codoping did not change the spinel structure and the electrochemical reaction mechanism of LTO. The electrochemical properties of LTO, especially the rate capability, were significantly improved by W^{6+} & Br^--codoping due to the increased electrical conductivity and Li^+ diffusion coefficient and correspondingly reduced electrochemical polarization during high rate charge/discharge process. The optimized composition of $Li_4Ti_{5-x}W_xO_{12-x}Br_x$ (x=0.05) exhibited the best rate capability, showing a high discharge capacity of 138.8 $mAh{\cdot}g^{-1}$and a capacity retention of 88.7% over 1000 cycles at 10 C rate. We believe that the strategy adopted in this work can be applied to develop other cathode materials with inferior electrical conductivity.

Acknowledgements

The authors are grateful for the financial support from China Postdoctoral Science Foundation (No. 2015M572379), the Hundred Talents Program of Chinese Academy of Sciences (CAS), "Gan-Po Talent 555" project of Jiangxi Province, Collaboration Project of CAS-Guangdong Province (2013B091300017), and Guangzhou Municipal Project for Science & Technology (201423/2014Y2-00219).

References

1 J. M. Tarascon and M. Armand, *Nature*, 2001, **414**, 359.
2 T. F. Yi, S. Y. Yang and Y. Xie, *J. Mater. Chem. A*, 2015, **3**, 5750.
3 Y. Q. Wang, L. Gu, Y. G. Guo, H. Li, X. Q. He, S. Tsukimoto, Y. Ikuhara and L. J. Wan, *J. Am. Chem. Soc.*, 2012, **134**, 7874.
4 J. L. Guo, W. H. Zuo, Y. J. Cai, S. M. Chen, S. J. Zhang and J. P. Liu, *J. Mater. Chem. A*, 2015, **3**, 4938.
5 Y. J. Sha, B. T. Zhao, R. Ran, R. Cai and Z. P. Shao, *J. Mater. Chem. A*, 2013, **1**, 13233.
6 L. Sun, J. P. Wang, K. L. Jiang and S. S. Fan, *J. Power Sources*, 2014, **248**, 265.
7 K. Song, D. H. Seo, M. R. Jo, Y. I. Kim, K. Kang and Y. M. Kang, *J. Phys. Chem. Lett.*, 2014, **5**, 1368.
8 Z. Q. Zhu, F. Y. Cheng and J. Chen, *J. Mater. Chem. A*, 2013, **1**, 9484.
9 D. Z. Kong, W. N. Ren, Y. S. Luo, Y. P. Yang and C. W. Cheng, *J. Mater. Chem. A*, 2014, **2**, 20221.
10 Z. H. Zhang, G. C. Li, H. R. Peng and K. Z. Chen, *J. Mater. Chem. A*, 2013, **1**, 15429.
11 Q. Y. Zhang, C. L. Zhang, B. Li, S. F. Kang, X. Li and Y. G. Wang, *Electrochim. Acta*, 2013, **98**, 146.
12 Y. J. Bai, C. Gong, N. Lun and Y. X. Qi, *J. Mater. Chem. A*, 2013, **1**, 89.
13 B. F. Wang, J. S. Wang, J. Cao, H. H. Ge and Y. F. Tang, *J. Power Sources*, 2014, **266**, 150.
14 T. F. Yi, S. Y. Yang, X. Y. Li, J. H. Yao, Y. R. Zhu and R. S. Zhu, *J. Power Sources*, 2014, **246**, 505.
15 H. Kaftelen, M. Tuncer, S. Y. Tu, S. Repp, H. Gocmez, R. Thomann, S. Weber and E. Erdem, *J. Mater. Chem. A*, 2013, **1**, 9973.
16 C. F. Lin, X. Y. Fan, Y. L. Xin, F. Q. Cheng, M. O. Lai, H. H. Zhou and L. Lu, *Nanoscale*, 2014, **6**, 6651.
17 L. Zhao, Y. S. Hu, H. Li, Z. Wang and L. Chen, *Adv. Mater.*, 2011, **23**, 1385.
18 P. S. Herle, B. Ellis, N. Coombs and L. F. Nazar, *Nature Mater.*, 2004, **3**, 147.
19 J. S. Huang, L. Yang, K. Y. Liu and Y. F. Tang, *J. Power Sources*, 2010, **195**, 5013.
20 D. Young, A. Ransil, R. Amin, L. Zheng and Y. M. Chiang, *Adv. Energy Mater.*, 2013, **3**, 1125.
21 H. Song, S. W. Yun, H. H. Chun, M. G. Kim, K. Y. Chung, H. S. Kim, B. W. Cho and Y. T. Kim, *Energy Environ. Sci.*, 2012, **5**, 9903.
22 Y. Ma, B. Ding, G. Ji and J. Y. Lee, *ACS Nano*, 2013, **7**, 10870.
23 C. F. Lin, M. O. Lai, L. Lu and H. H. Zhou, *J. Phys. Chem. C*, 2014, **118**, 14246.
24 Q. Y. Zhang, M. G. Verde, J. K. Seo, X. Li and Y.S. Meng, *J. Power Sources*, 2015, **280**, 355.
25 M. D. Ji, Y. L. Xu, Z. Zhao, H. Zhang, D. Liu, C. J. Zhao, X. Z. Qian and C. H. Zhao, *J. Power Sources*, 2014, **263**, 296.
26 S. H. Huang, Z. Y. Wen, Z. H. Gu and X. J. Zhu, *Electrochim. Acta*, 2005, **50**, 4057.
27 C. X. Qiu, Z. Z. Yuan, L. Liu, S. J. Cheng and J. C. Liu, *Chin. J. Chem.*, 2013, **31**, 819.
28 A. Y. Shenouda and K. R. Murali, *J. Power Sources*, 2008, **176**, 332.
29 Q. Y. Zhang, C.L. Zhang, B. Li, D.D. Jiang, S.F. Kang, X. Li and Y.G. Wang, *Electrochim. Acta*, 2013, **107**, 139.
30 J. Q. Wang, Z. Z. Yang, W. H. Li, X. W. Zhong, L. Gu, Y. Yu, J. Power Sources, 2014, **266**, 323.
31 Y. L. Qi, Y. D. Huang, D. Z. Jia, S. J. Bao and Z. P. Guo, *Electrochim. Acta*, 2009, **54**, 4772.
32 G. Kresse and J. Hafner, *Phys. Rev. B*, 1993, **47**, 558.
33 S. Q. Shi, C. Y. Ouyang, D. S. Wang, Z. X. Wang, L. Q. Chen and X. J. Huang, *Solid State Commun.*, 2003, **126**, 531.
34 C. Y. Ouyang, S. Q. Shi, Z. X. Wang, H. Li, X. J. Huang and L. Q. Chen, *Europhys. Lett.*, 2004, **67**, 28.
35 J. P. Perdew, J. A. Chevary, S. H. Vosko, K. A. Jackson, M. R. Pederson, D. J. Singh and C. Fiolhais, *Phys. Rev. B*, 1992, **46**, 6671.
36 A. Deschanvres, B. Raveau and Z. Sekkal, *Mater. Res. Bull.*, 1971, **6**, 699.
37 B. Tian, H. Xiang, L. Zhang, Z. Li and H. Wang, *J. Solid State Electrochem.*, 2012, **16**, 205.
38 R. B. Hadjean and J.P. P. Ramos, *Chem. Rev.*, 2010, **110**, 1278.
39 Y. Shi, J. Gao, H. D. Abruňa, H. K. Liu, H. J. Li, J. Z. Wang and Y. P. Wu, *Nano Energy*, 2014, **8**, 297.
40 C. C. Yang, H. C. Hu, S. J. Lin and W. C. Chien, *J. Power Sources*, 2014, **258**, 424.
41 M.V. P. Jarman, P.J. Hendra and R.J. Lehnert, *Vib. Spectrosc.*, 1996, **12**, 257.

42 H.G. Jung, S.T. Myung, C.S. Yoon, S.B. Son, K.H. Oh, K. Amine, B. Scrosati and Y.K. Sun, *Energy Environ. Sci.*, 2011, **4**, 1345.
43 T.F. Yi, Y. Xie, Q. Wu, H. Liu, L. Jiang, M. Ye and R. Zhu, *J. Power Sources*, 2012, **214**, 220.
44 J. Wolfenstine and J.L. Allen, *J. Power Sources*, 2008, **180**, 582.
45 Y. Wang, H. Liu, K. Wang, H. Eiji, Y. Wang and H. Zhou, *J. Mater. Chem.*, 2009, **19**, 6789.
46 H. L. Zhao, Y. Li, Z. Z. Zhu, J. Lin, Z. H. Tian and R. L. Wang, *Electrochim. Acta*, 2008, **53**, 7079.

Figures

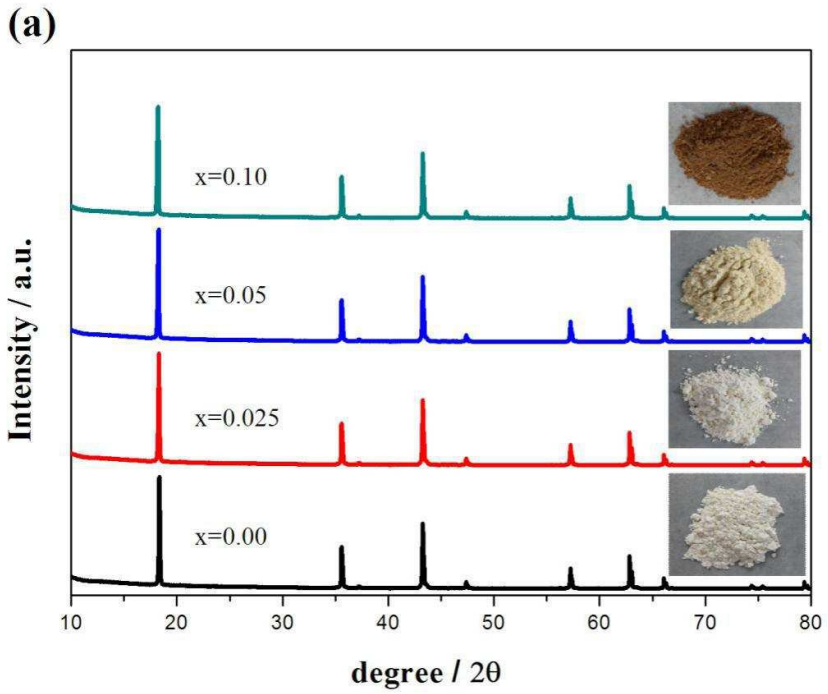

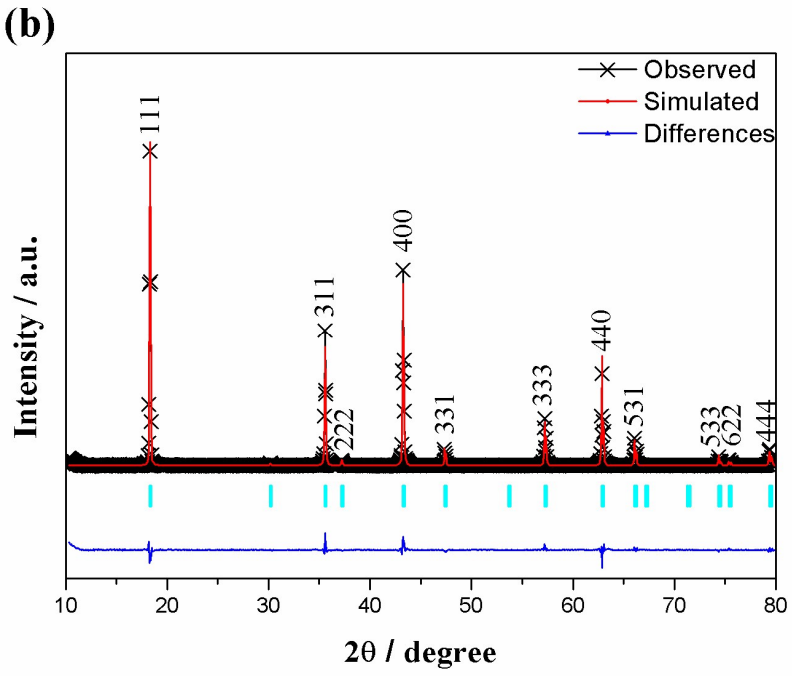

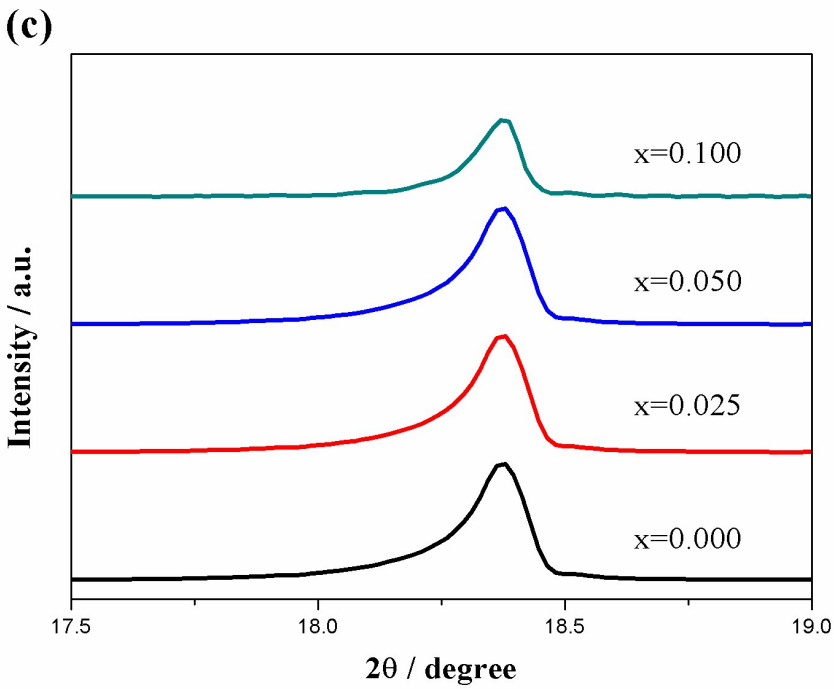

Fig. 1. (a) XRD patterns and colors of as-prepared $Li_4Ti_{5-x}W_xO_{12-x}Br_x$ (x=0, 0.025, 0.05, 0.10) samples, (b) representative Rietveld refinement when x=0.05 and (c) enlarged (1 1 1) peaks

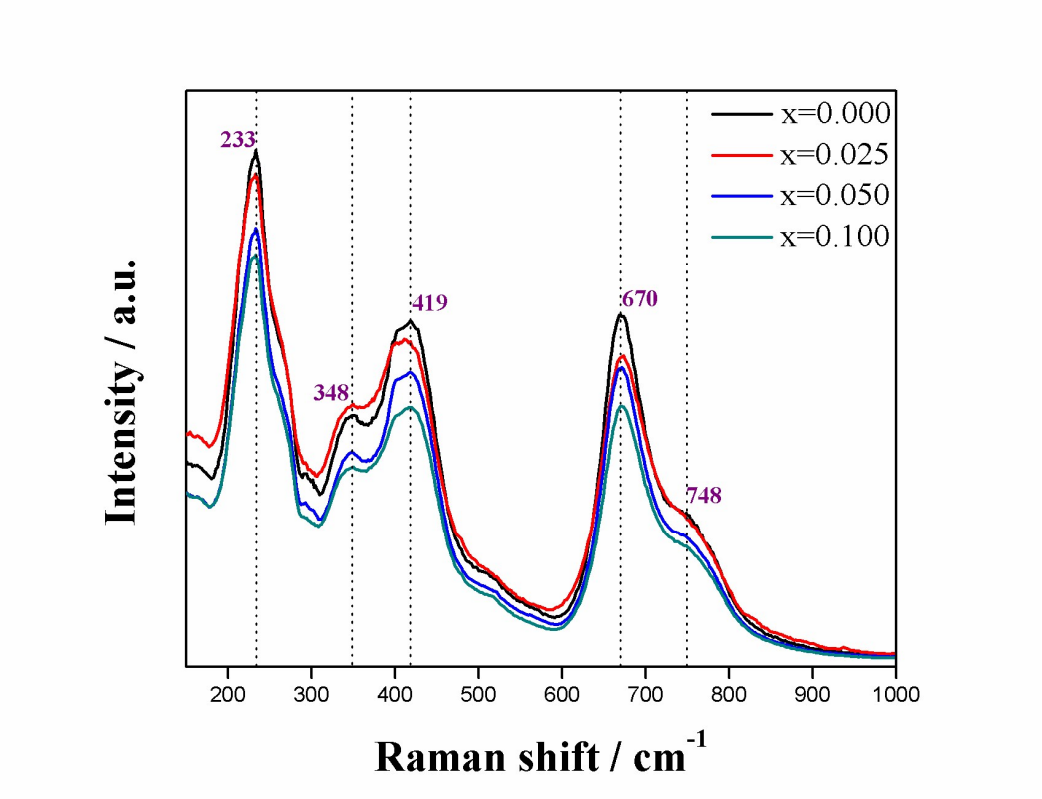

Fig.2. Raman spectra of all as-prepared samples.

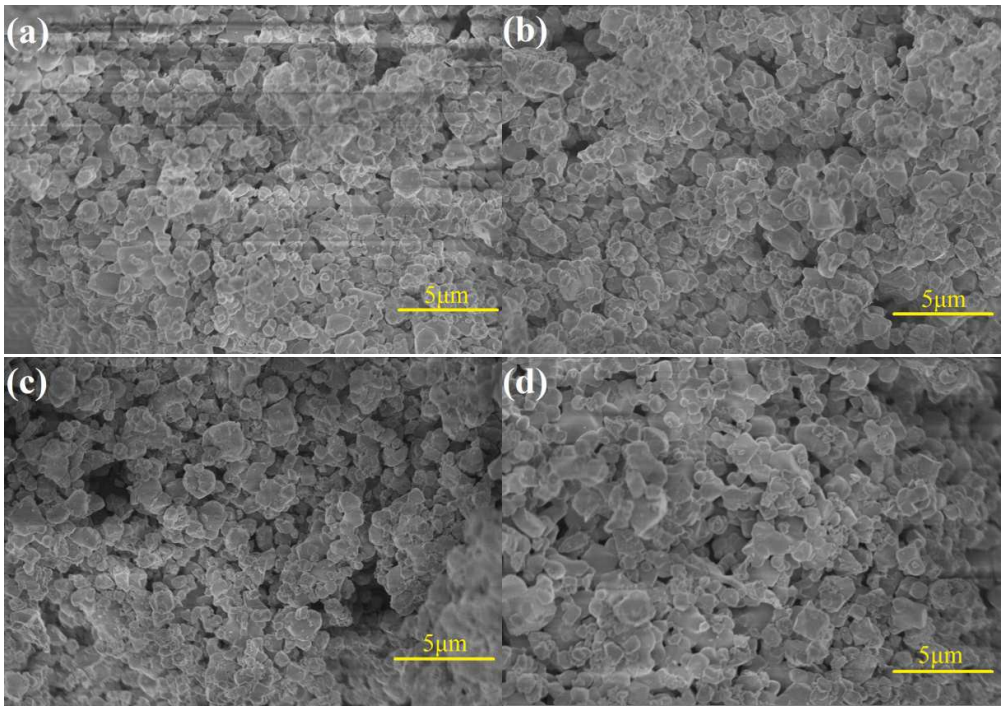

Fig. 3. SEM images of $Li_4Ti_{5-x}W_xO_{12-x}Br_x$ with (a) x=0, (b) x=0.025, (c) x=0.05, and

(d) x=0.10.

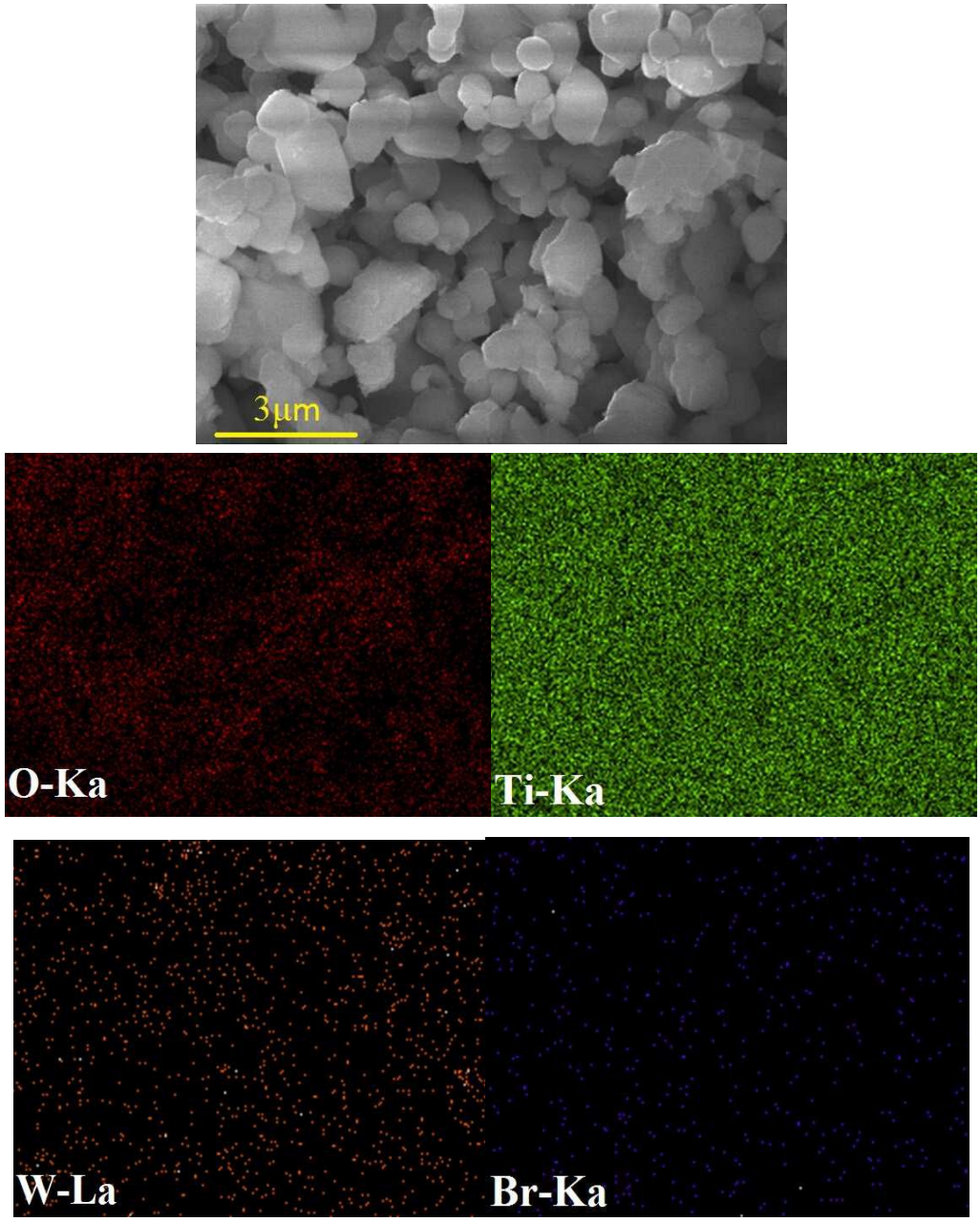

Fig. 4.EDS elemental mapping (O, Ti, W and Br) for the selected area of the sample $Li_4Ti_{4.95}W_{0.05}O_{11.95}Br_{0.05}$. The SEM image (top) shows the selected area corresponding to the elemental mapping of the codoped LTO particle when x=0.05.

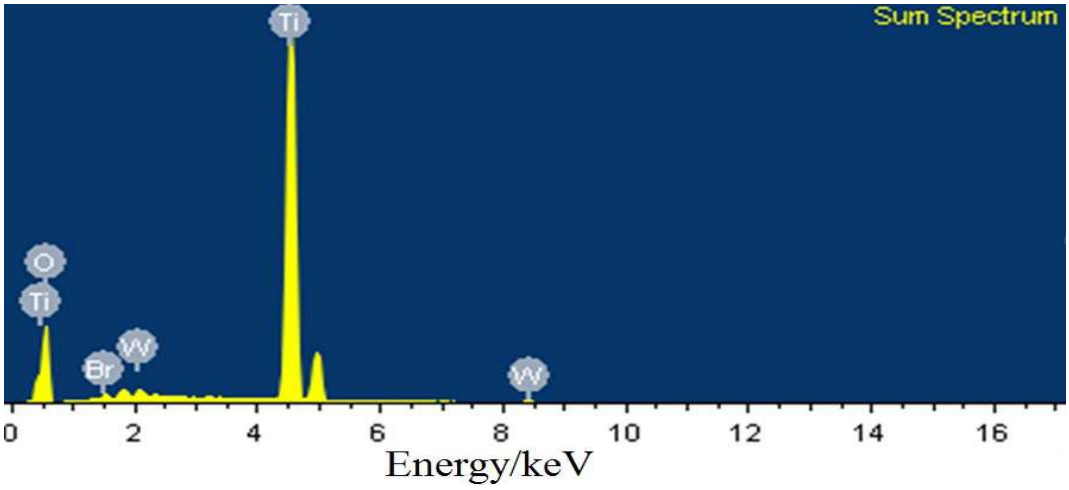

Fig. 5. EDX spectrum of the surface of $Li_4Ti_{4.95}W_{0.05}O_{11.95}Br_{0.05}$ material (x=0.05).

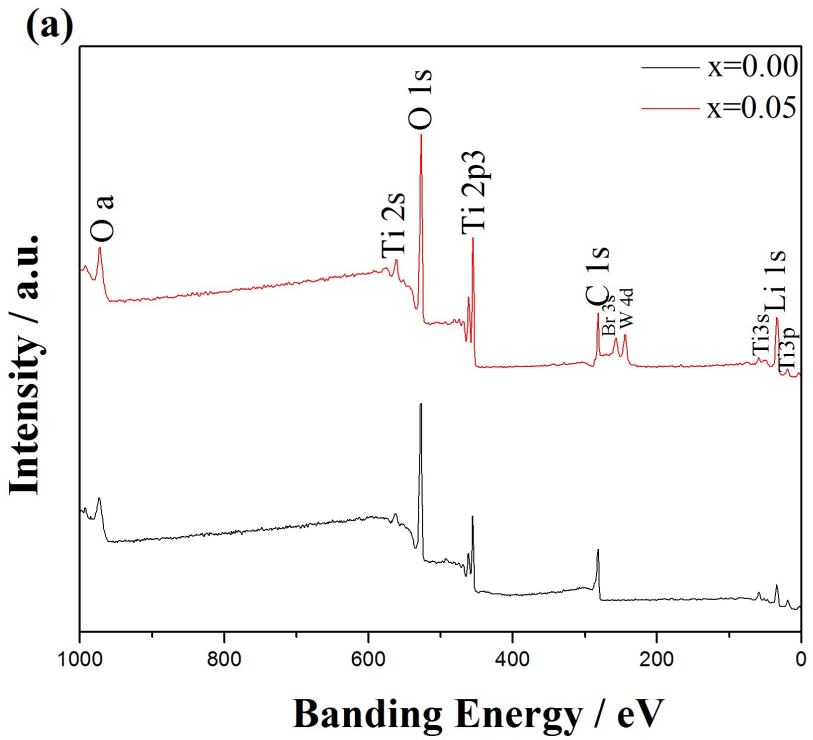

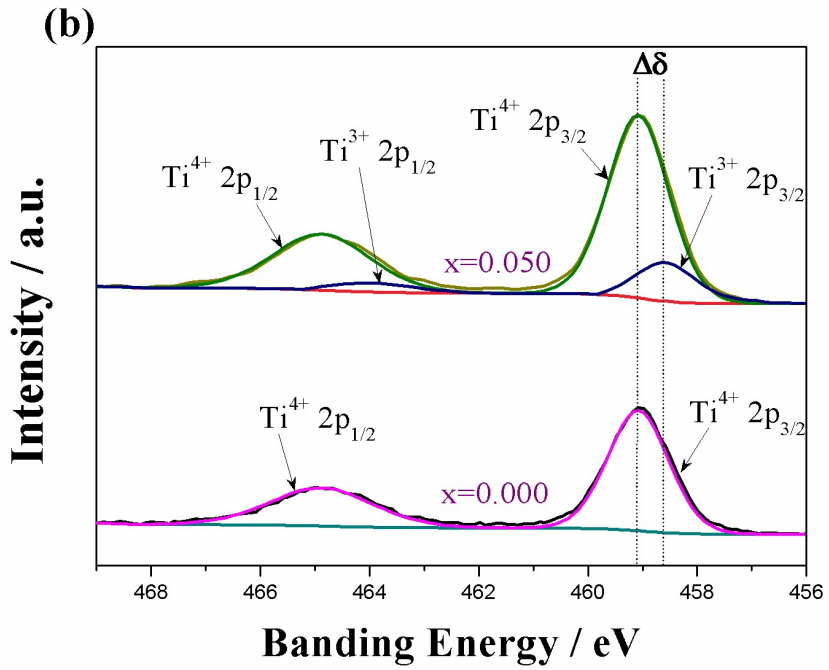

Fig.6. (a) The XPS survey spectra and (b) HR XPS spectra of Ti 2p peaks for $Li_4Ti_{5-x}W_xO_{12-x}Br_x$ (x= 0, 0.05).

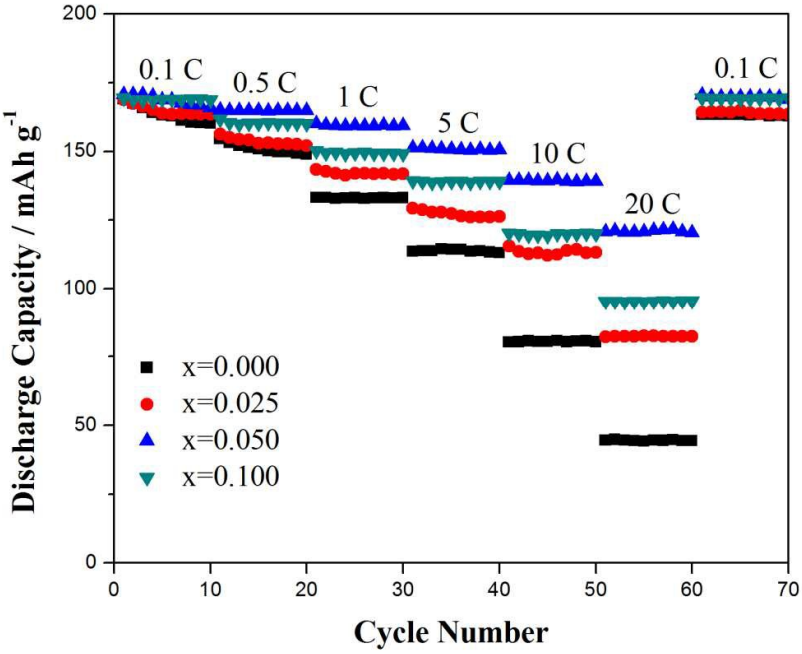

Fig. 7. Cyclic performance of the $Li_4Ti_{5-x}W_xO_{12-x}Br_x$ (x=0, 0.025, 0.05, 0.10) samples at various current rates from 0.1 to 20 C.

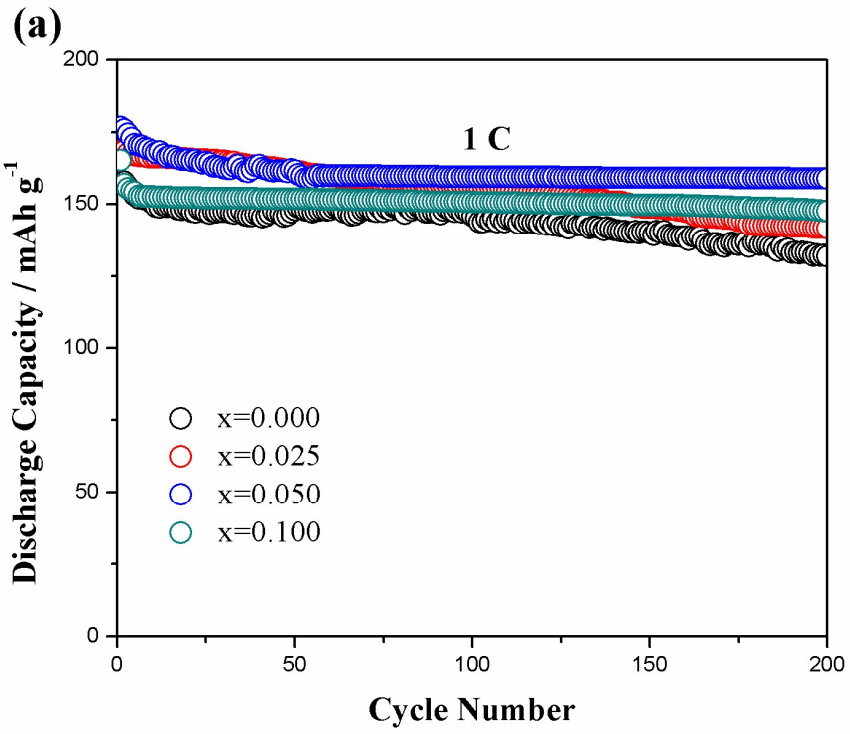

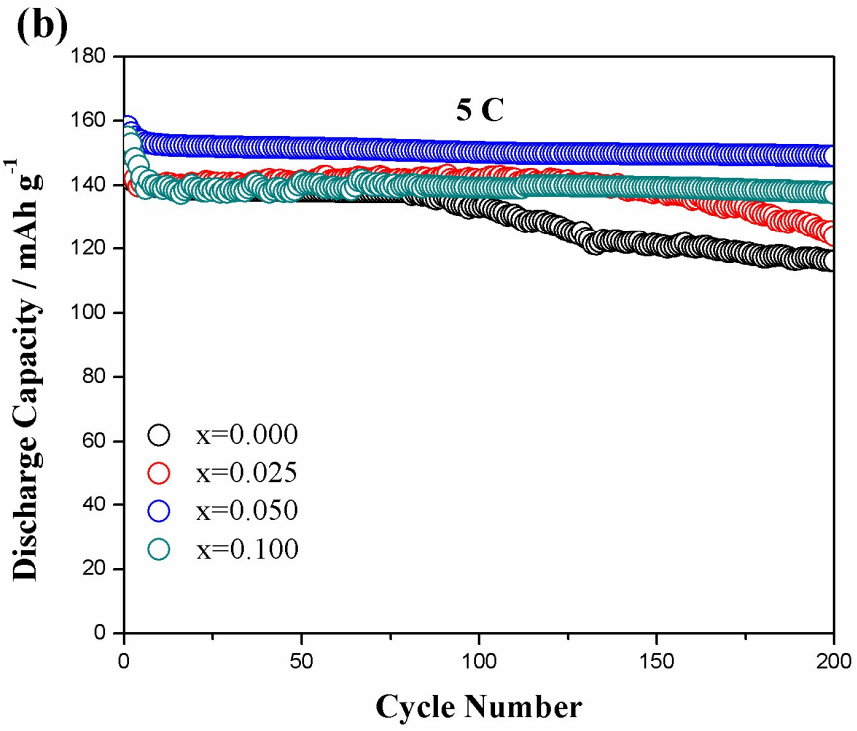

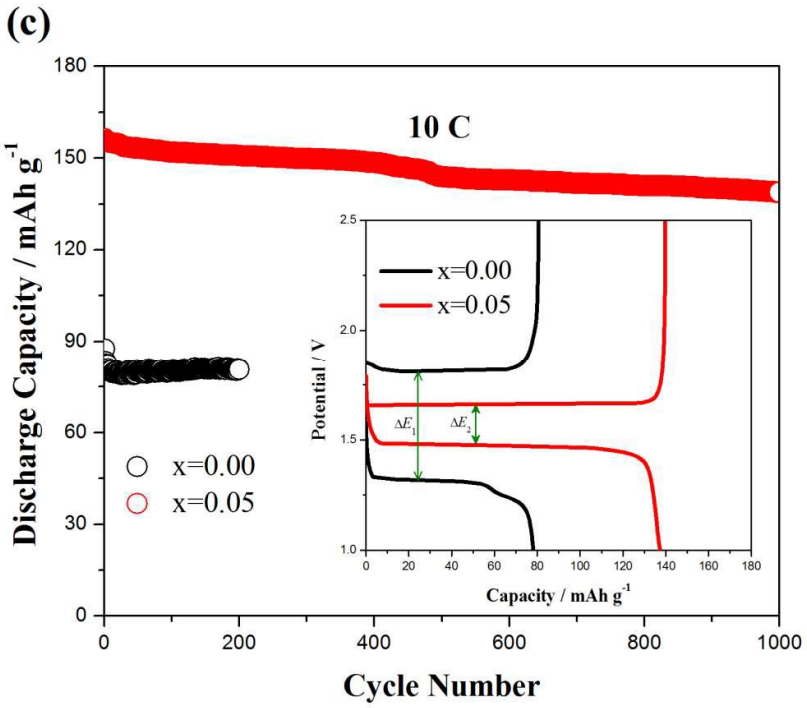

Fig. 8. Cyclic performance for $Li_4Ti_{5-x}W_xO_{12-x}Br_x$ (x=0, 0.025, 0.05, 0.10) at different rates, (a) 1C, (b) 5C and (c) 10C.

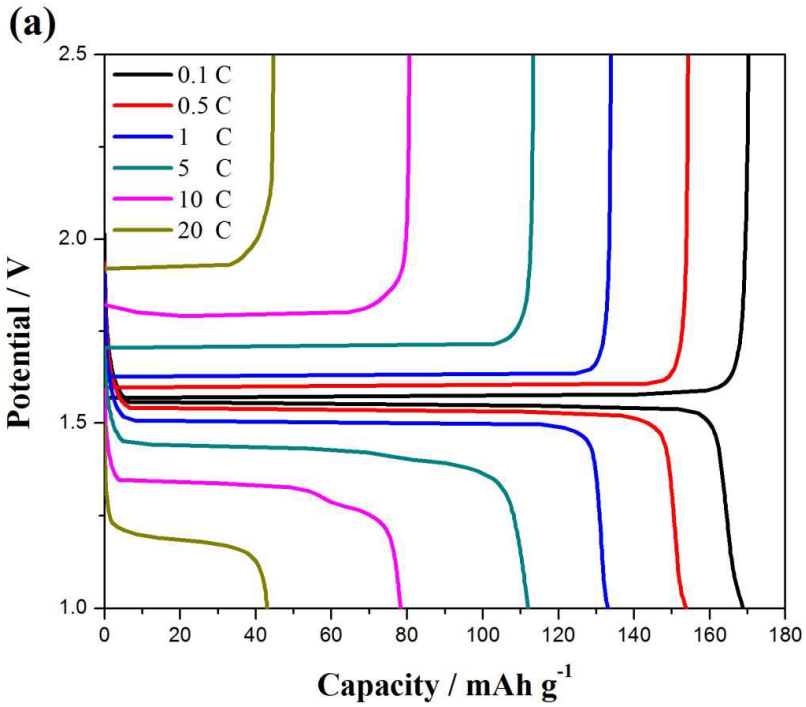

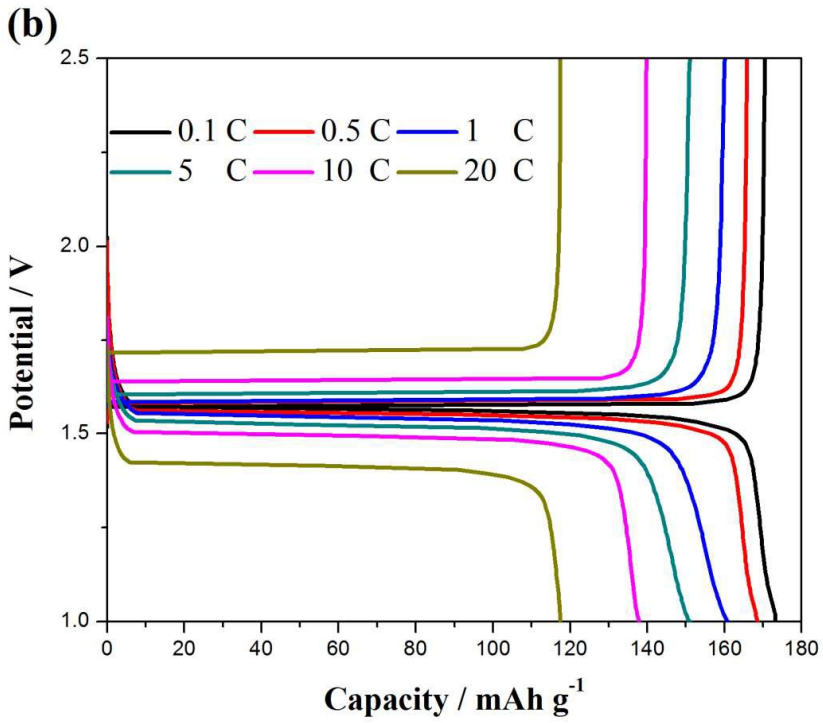

Fig. 9. Potential-Capacity curves of (a) $Li_4Ti_5O_{12}$ and (b) $Li_4Ti_{4.95}W_{0.05}O_{11.95}Br_{0.05}$ electrodes at various current rates.

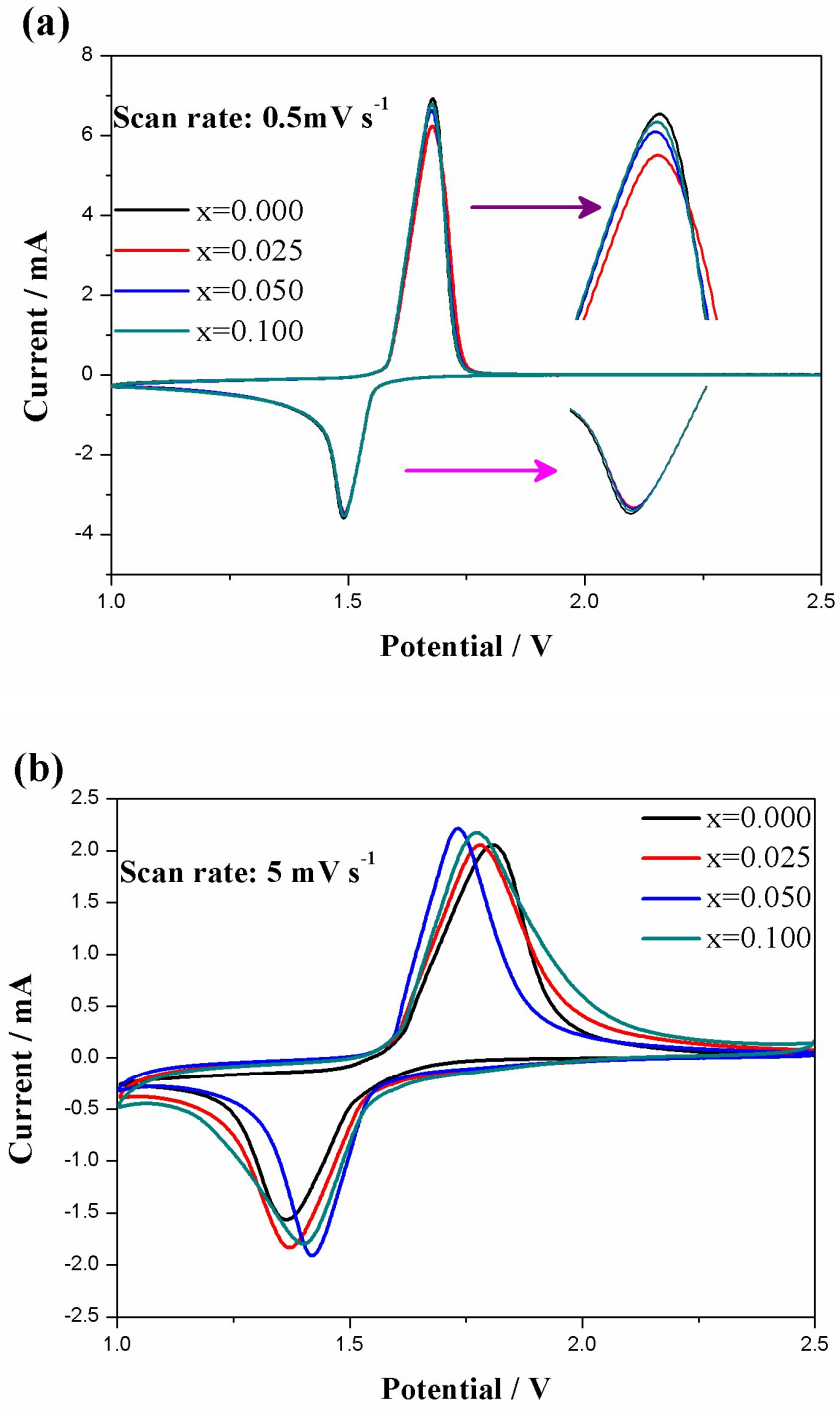

Fig. 10. Cyclic voltammograms of the $Li_4Ti_{5-x}W_xO_{12-x}Br_x$ (x=0, 0.025, 0.05, 0.10) at different scan rates of (a) 0.5 $mV \cdot s^{-1}$and (b) 5 $mV \cdot s^{-1}$.

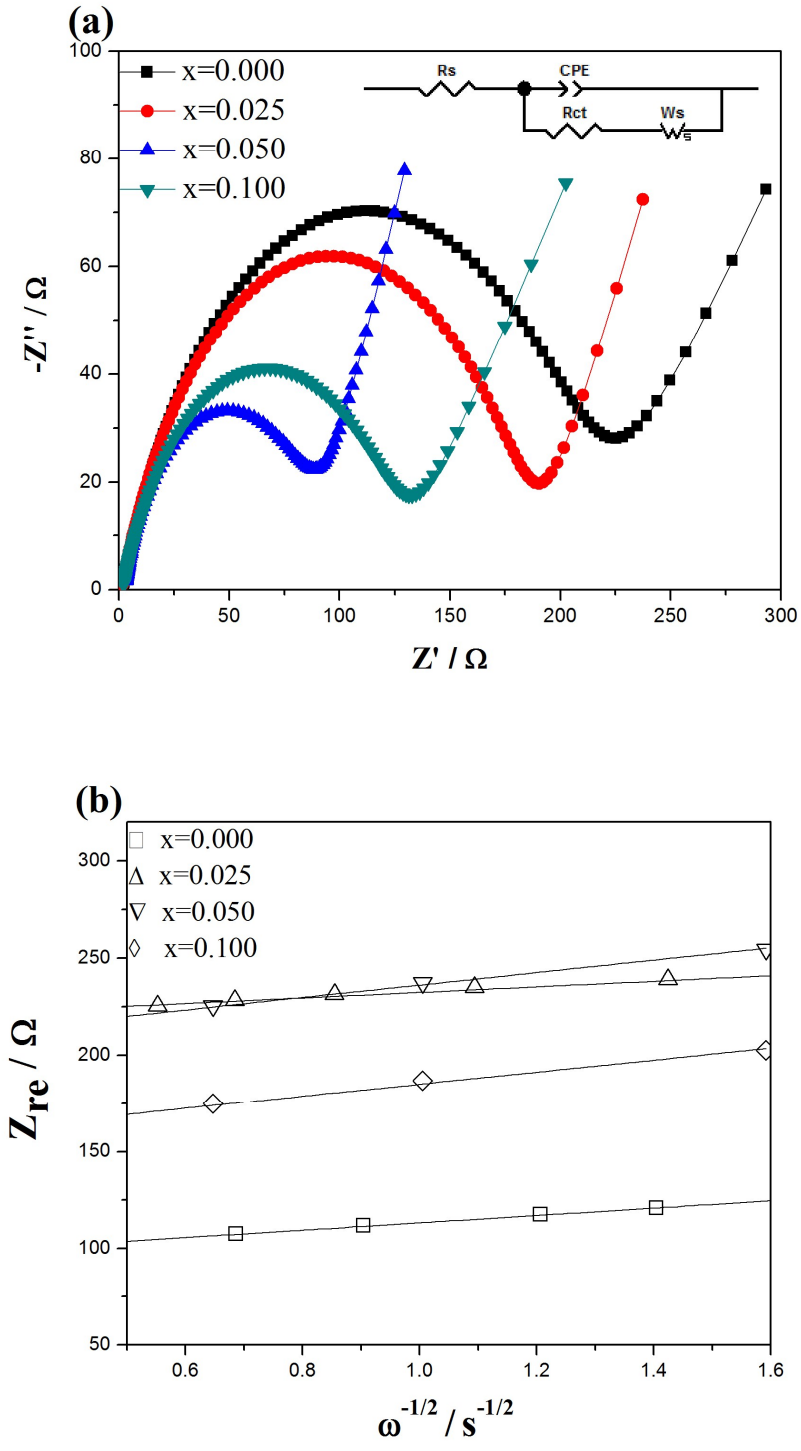

Fig. 11. (a) AC impedance spectra of the $Li_4Ti_{5-x}W_xO_{12-x}Br_x$ (x=0, 0.025, 0.050, 0.100) electrodes at the voltage of 1.55 V and (b) the relationship between the real impedance and the low frequencies of pristine and codoped LTO.

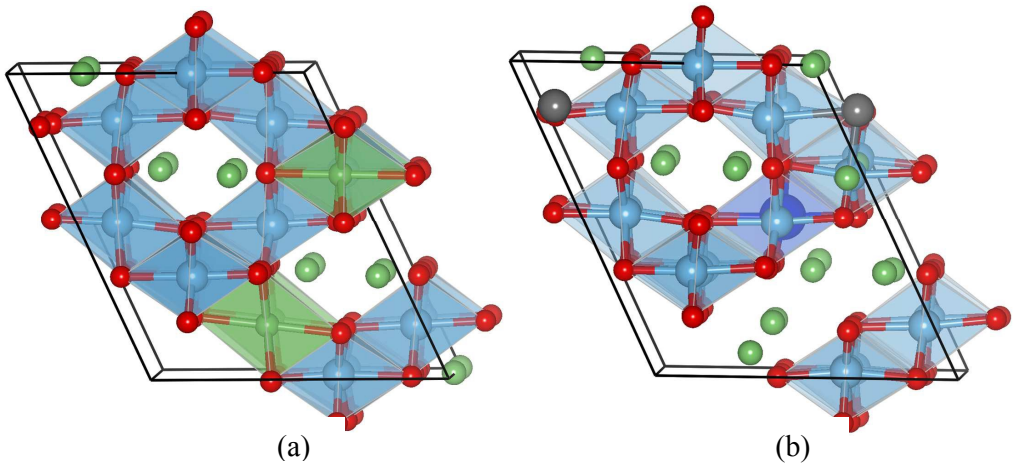

Fig. 12. Lattice models of (a) $Li_4Ti_5O_{12}$ and (b) $Li_{16}Ti_{19}W_1O_{47}Br_1$ with correct stoichiometry. Herein, red sphere represents oxygen atom; blue sphere represents titanium atom; green spheres represents lithium atom; purple sphere represents bromine atom; gray sphere represents tungsten atom.

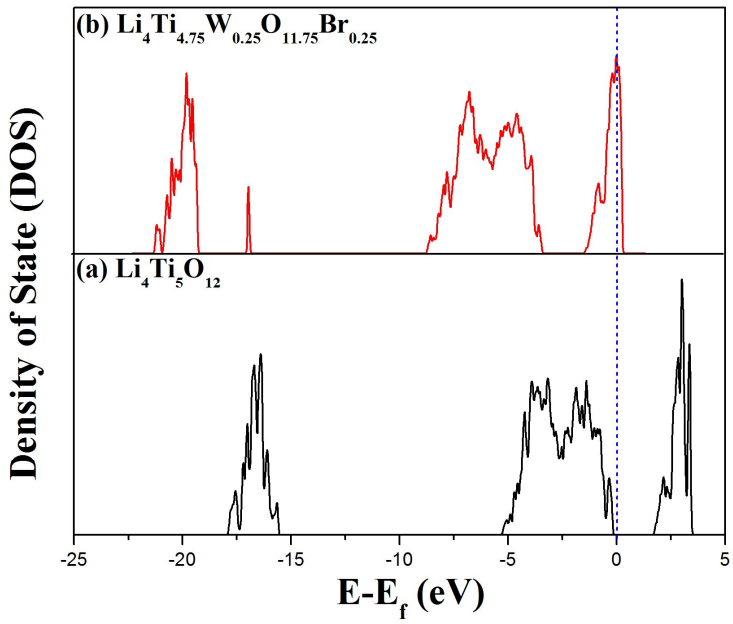

Fig. 13. Density of states (DOS) of (a) $Li_4Ti_{4.75}W_{0.25}O_{11.75}Br_{0.25}$ and (b) $Li_4Ti_5O_{12}$, the Fermi energy is normalized to 0 eV.

Tables

Table 1

The final chemical composition of the W&Br-codoped spinel LTO.

Sample	Nominal formula	Composition(wt.%)					Final composition
		Li	Ti	W	O	Br	
x=0.000	$Li_4Ti_5O_{12}$	6.05	52.15	0.00	41.80	0.00	$Li_4Ti_5O_{12}$
x=0.025	$Li_4Ti_{4.975}W_{0.025}O_{11.975}Br_{0.025}$	5.99	51.41	0.91	41.33	0.36	$Li_4Ti_{4.977}W_{0.023}O_{11.979}Br_{0.021}$
x=0.050	$Li_4Ti_{4.95}W_{0.05}O_{11.95}Br_{0.05}$	5.92	50.56	1.96	40.79	0.77	$Li_4Ti_{4.95}W_{0.05}O_{11.955}Br_{0.045}$
x=0.100	$Li_4Ti_{4.9}W_{0.1}O_{11.9}Br_{0.1}$	5.80	49.04	3.84	39.81	1.50	$Li_4Ti_{4.9}W_{0.1}O_{11.91}Br_{0.09}$

Table 2

The lattice parameter of $Li_4Ti_{5-x}W_xO_{12-x}Br_x$ (x= 0, 0.025, 0.05, 0.10) samples.

Sample	α / nm
x=0.000	0.8357
x=0.025	0.8362
x=0.050	0.8368
x=0.100	0.8375

Table 3

Potential differences between anodic and cathodic peaks of the $Li_4Ti_{5-x}W_xO_{12-x}Br_x$ (x=0, 0.025, 0.05, 0.1) electrodes for the fresh cells at different scan rates.

Scan rate	0.5 mV·s^{-1}			5mV·s^{-1}		
x	φ_a/V	φ_c/V	ΔE/mV	φ_a/V	φ_c/V	ΔE/mV
0.000	1.679	1.490	189	1.808	1.361	447
0.025	1.677	1.492	185	1.780	1.371	409
0.050	1.676	1.492	184	1.733	1.418	315
0.100	1.677	1.491	186	1.770	1.399	371

φ_a─ Anodic peak; φ_c─ Cathodic peak; ΔE─ φ_a - φ_c.

Table 4 Impedance parameters of $Li_4Ti_{5-x}W_xO_{12-x}Br_x$ (x=0, 0.025, 0.050, and 0.100) electrodes.

Sample	R_s/Ω	R_{ct}/Ω	σ_w/Ω·cm^2·s$^{0.5}$	D/cm^2·s
x=0.000	1.895	213.2	42.10	2.98x10^{-13}
x=0.025	1.766	187.2	31.16	5.66x10^{-13}
x=0.050	1.041	88.7	14.32	2.68x10^{-12}
x=0.100	1.481	126.0	18.97	1.51x10^{-12}